On the use of recurrent neural networks for fast and accurate non-uniform gas radiation modeling

Frédéric André, Céline Cornet, Cindy Delage, Philippe Dubuisson, Mathieu Galtier

▶ **To cite this version:**

Frédéric André, Céline Cornet, Cindy Delage, Philippe Dubuisson, Mathieu Galtier. On the use of recurrent neural networks for fast and accurate non-uniform gas radiation modeling. Journal of Quantitative Spectroscopy and Radiative Transfer, 2022, 293, pp.108371. 10.1016/j.jqsrt.2022.108371 . hal-03826189

HAL Id: hal-03826189
https://hal.science/hal-03826189v1

Submitted on 13 Nov 2023

HAL is a multi-disciplinary open access archive for the deposit and dissemination of scientific research documents, whether they are published or not. The documents may come from teaching and research institutions in France or abroad, or from public or private research centers.

L'archive ouverte pluridisciplinaire **HAL**, est destinée au dépôt et à la diffusion de documents scientifiques de niveau recherche, publiés ou non, émanant des établissements d'enseignement et de recherche français ou étrangers, des laboratoires publics ou privés.

ON THE USE OF RECURRENT NEURAL NETWORKS FOR FAST AND ACCURATE NON-UNIFORM GAS RADIATION MODELING

Frédéric ANDRE[a,*], Céline CORNET[b], Cindy DELAGE[a], Philippe DUBUISSON[b], Mathieu GALTIER[a]

[a] Univ Lyon, CNRS, INSA-Lyon, Université Claude Bernard Lyon 1, CETHIL UMR 5008, F-69621 Villeurbanne, France

[b] Univ Lille, CNRS, UMR 8518 - LOA, F-59000 Lille, France

- Corresponding author

Email adress: frederic.andre@insa-lyon .fr

ABSTRACT This paper focuses on the construction of a fast though accurate gas radiation model based on a Recurrent Neural Network (RNN) formulation. The model is founded on recent works in which a solution to a non-uniform technique proposed by Godson in the 50s was derived explicitly. The method uses a non-linear transformation of a set of physical / geometrical paths, directly related to a non-uniform path which is first discretized into uniform sub-layers, into a sequence of equivalent absorption lengths. This process, studied thoroughly within the frame of the development of the ℓ-distribution approach, can be naturally handled using an algorithm that takes the form of an RNN model. The method is assessed against LBL calculations in non-uniform high temperature gaseous media and found to provide more accurate results than a CKD (Correlated K-Distribution) model with 16 gray gases. This paper is the first to suggest an RNN to treat radiative transfer in non-uniform gaseous media. Moreover, all the weights involved in the RNN have a clear physical meaning so that the structure of the RNN can be readily interpreted, avoiding the black box disadvantage of most brute force machine learning strategies.

Keywords: gas radiation, Godson, ℓ-distribution, Propagative Form, Recurrent Neural Network.

1. INTRODUCTION

There have been several attempts in the recent literature to apply methods based on Machine Learning, including artificial neural networks, to radiative transfer and gas radiation modeling. For instance, refs. [1,2], that are not strictly restricted to gaseous media as considered in the present work, are two examples of application of machine learning techniques to solve the RTE. More related to gas radiation, in ref. [3], a machine learning strategy is used to replace look-up tables in the Full Spectrum Correlated-k (FSCK) method. Applying neural networks instead of look-up tables was shown to reduce significantly the overall computational cost of the FSCK method (both in terms of memory requirements and computation time) without modifying the quality of the FSCK model itself. More recently, in ref. [4], a feedforward neural network strategy is described to model directly gas path transmissivities in atmospheric applications. Errors of a few percent of the full transmission scale, *i.e.* [0,1], were obtained in this work over non-uniform atmospheric paths.

The present work is an extension of a recent paper [5] in which a reformulation of the ℓ-distribution approach in terms of neural network was mentioned but not derived in full details. The aim of the present paper is to describe this formulation. The modeling strategy is based on previous works in which explicit functional forms were derived for the solution of Godson's implicit equation [6]. This solution is shown here to be naturally written in a Recurrent Neural Network form (RNN) involving Exponential Linear Units (ELU) as activation functions. The present method is, to the best of the authors' knowledge, the first to consider RNNs to model non-uniform gas path transmissivities. Compared to existing machine learning strategies, that apply brute force neural network methods, the present formulation provides an RNN whose coefficients are fully based on physical modeling. The interpretability of all coefficients appearing in the RNN model is thus possible, as compared with other methods for which neural networks mostly act as black boxes. The modeling strategy is applied here in the context of high temperatures but it can be extended to atmospheric paths with minor modifications. It bridges an old idea (from the 50s) with modern algorithmic developments in probably one of its optimal ways.

Almost 70 years ago, in 1953 [6], Warren L. Godson introduced three methods to extend uniform gas radiation models from uniform (ref. [6] was limited to Elssasser's model) to

non-uniform configurations. Among these methods, one of them led to the widely used Curtis-Godson (CG) approximation, fully derived in 1955 within the frame of the statistical narrow band model for Lorentz lines [7]. The great success of the CG approximation has almost obliterated the potential of the two other methods proposed in [6], even if one of them was shown from the early beginning to be superior to CG. Deficiencies of the CG approximation in cases of highly non-uniform configurations were observed and studied in the 70s, leading to the Lindquist-Simmons (LS) approximation [8]. This method suggests a new starting point for the treatment of non-uniformities based on the derivative of the transmission function with respect to the gas path length. The LS method usually provides a more accurate and physical treatment of non-uniform paths than CG [9], but introduces some asymmetries in the non-uniform model. A compendium of existing versions of the CG and LS approximations can be found in [9,10].

Godson's method was reintroduced in the 70s by Weinreb and Neuendorffer [11], but instead of the Elsasser's model used in [6], a polynomial approximation of transmissivities was applied. Several direct applications of Godson's method to atmospheric configurations can be found, under the names Pseudo Mass Approximation (PMA) or Emissivity Growth Approximation (EGA) in refs. [12-14]. In the high temperature literature, Modest [15] uses a technique similar to Godson's method within the frame of k-distribution models and calls it the Scaled-k method. No reference to Godson's work is made in ref. [15]. All these works (PMA, EGA, Scaled-k) have two elements in common. The first one is that Godson's method is found to be very accurate when assessed against LBL calculations. When such results are available, Godson's method is also found to be as accurate (in most cases more accurate) than the widely used CKD method. The second one is that no one of them have attempted to justify physically the reasons that could explain the accuracy of this non-uniform method.

The development of the ℓ-distribution approach [16] has led recently to the concept of quasi-scaled spectra. This assumption, which is a physical/statistical model of relationship between spectra in distinct thermophysical states, was introduced in ref. [17]. It allows understanding most of the properties of Godson's method. Among them, it provides an explanation of the asymmetry of Godson's method in strongly non-uniform configurations, a property noticed from the early beginning, but almost absent from all

the papers cited previously [12-15]. This problem of asymmetry is studied in depths in refs. [5,17].

The three techniques (Godson's, Scaled-k and ℓ-distribution methods) share similarities but are fundamentally different. For instance, the Scaled-k method requires the definition of a reference state of the gas whereas Godson's and ℓ-distribution methods do not. The Scaled-k and Godson's methods rely on iterative techniques to find a solution of the model's implicit equation (see Eq. (7) later in the paper), whereas in ℓ-distribution a semi-analytical solution of the same equation is used. Consequently, the approach used in ℓ-distribution allows treating non-uniform paths very efficiently, compared to the two other iterative methods. In the Scaled-k and Godson's methods, the implicit equation used to define an effective scaling factor is introduced without reference to any physical model. In ℓ-distribution, on the other hand, the implicit equation is founded on the assumption of quasi-scaling of gas spectra in distinct thermophysical states as noticed previously. Additional details on how the quasi-scaling property connects with Godson's method are provided later in this paper.

The ℓ-distribution method was up to now mostly studied in its Archimedean copula version. The main advantage of such a formalism is to help understanding and controlling the properties of the non-uniform model and its impact on the calculation of transmissivities of non-uniform paths using known results from copula theory. Its main disadvantage is to make the model probably hard to understand at first sight for possible users not familiar with the concept of copula and/or gas radiation modeling. Nevertheless, recently, we have shown [5] that the copula formulation of the ℓ-distribution approach can be equivalently written in a propagative form, in which only relationships between equivalent absorption lengths are used. The possibility to reformulate the method in a neural network version was also suggested in the same reference. The same mathematical results as used in the copula version of the model can be applied in the propagative formulation, as they are rigorously equivalent. However, the propagative version is probably simpler to understand. This propagative form, including its recurrent neural network formulation, is the main focus of the present work.

The paper is structured as follows. In the second section, the main assumptions used to treat non-uniform paths in the ℓ-distribution approach are detailed. This allows obtaining a definition of effective scaling factors (that is to say scaling coefficients that depend on the gas path length) that coincides with Godson's method. The third section is devoted to an approximation of the quantities used in the ℓ-distribution method using simple relationships. The resulting uniform method, that involves a three coefficients transmission model, is described and assessed against LBL calculations. The same uniform cases as used in ref. [18] are treated to illustrate the quality of the parameterization. The fourth section is devoted to a reformulation of the key elements of Section 3 in terms of recurrent neural networks. As will be shown, the propagative version of the ℓ-distribution approach can be naturally written in a neural form using Exponential Linear Units (ELU) as activation functions without losing its physical interpretation. This reformulation, which is the main result of the present work, provides a proof of the relevance of application of RNN structures for non-uniform gas radiation modeling.

This work, even if it is mostly restricted to a simplified though very accurate model and not to real LBL datasets, is the first to suggest an RNN as a non-uniform gas model. It bridges physics and statistical/machine learning points of view in probably one of its optimal ways.

2. FROM SCALED / QUASI-SCALED SPECTRA TO GODSON'S METHOD

The concept of scaled spectra is among the most important ones in non-uniform gas radiation modeling. Even Correlated *k*-distribution (C*k* / CKD) methods rely on this assumption, although the scaling coefficient is not in this case a constant for all values of the absorption coefficient, but depends on it directly. Scaling assumes a linear relationship between gas spectra in distinct thermophysical states, a property that is obviously verified at LBL scale for single wavenumbers.

The hypothesis of scaled spectra assumes the existence of a constant coefficient, written from now on U, such that the spectral absorption coefficients of the gas in two thermophysical states (subscripts 1 and 2) are related by the linear relationship:

$$\kappa_{\nu,2} = U \cdot \kappa_{\nu,1} \tag{1}$$

When gas spectra are scaled, one has for any gas path length L:

$$\tau_2^{\Delta\nu}(L) = \frac{1}{\Delta\nu} \cdot \int_{\Delta\nu} \exp\left(-\kappa_{\nu,2}\, L\right)\, d\nu = \frac{1}{\Delta\nu} \cdot \int_{\Delta\nu} \exp\left(-U \cdot \kappa_{\nu,1}\, L\right)\, d\nu = \tau_1^{\Delta\nu}(U \cdot L) \tag{2}$$

The band averaged transmissivity of a non-uniform path in the gas (length L_1 in state 1 and L_2 in state 2) is then:

$$\tau_{12}^{\Delta\nu}(L_1, L_2) = \frac{1}{\Delta\nu} \cdot \int_{\Delta\nu} \exp\left(-\kappa_{\nu,1}\, L_1 - \kappa_{\nu,2}\, L_2\right)\, d\nu = \tau_1^{\Delta\nu}(L_1 + U \cdot L_2) \tag{3}$$

A similar relationship can be obtained if one considers *n* scaled spectra.

For the analysis of more general situations for which gas spectra are not truly scaled, a slight reformulation of the scaled model is required. It is provided below.

As band averaged transmissivities are strictly decreasing functions of pathlengths over absorbing bands that do not contain transparency regions of the gas, they are invertible. This means that one can define, for any transmission function, its inverse ℓ. This is the main principle of the ℓ-distribution approach. Using this inverse ℓ, one can rewrite Eq. (3) in two equivalent forms:

- Archimedean copula C_{11} version [5,19,20]:

$$\tau_{12}^{\Delta\nu}(L_1,L_2)=C_{11}\left[\tau_1^{\Delta\nu}(L_1),\tau_2^{\Delta\nu}(L_2)\right]\ \text{where: } C_{11}(X,Y)=\frac{1}{\Delta\nu}\cdot\int_{\Delta\nu}\exp\left[-\kappa_{\nu,1}\,\ell_1(X)-\kappa_{\nu,1}\,\ell_1(Y)\right]\,d\nu \tag{4}$$

- Propagative version [5]:

$$\tau_{12}^{\Delta\nu}(L_1,L_2)=\tau_1^{\Delta\nu}(L_{12})\ \text{where: } L_{12}=L_1+U\cdot L_2=\ell_1\,\mathrm{o}\,\tau_1^{\Delta\nu}(L_1)+\ell_1\,\mathrm{o}\,\tau_2^{\Delta\nu}(L_2) \tag{5}$$

In Eq. (5), the symbol "o" represents the functional composition, *i.e.*, given two functions f and g one has $f\,\mathrm{o}\,g(x)=f\left[g(x)\right]$. In the case of truly scaled gas spectra, all three formulations provided by Eqs. (3-5) are rigorously equivalent. These relationships can be readily extended to any n layer non-uniform path and remain exact as soon as all gas spectra encountered along the non-uniform path are rigorously scaled.

In practice, gas spectra are not perfectly scaled. However, in the case of small gradients of temperature or pressure, it was shown in ref. [17] that real gas spectra can be considered as quasi-scaled, i.e., given two distinct spectra, it is reasonable to assume that the two transmission functions can be connected to each other by:

$$\tau_2^{\Delta\nu}(L)=\int_0^{+\infty}\tau_1^{\Delta\nu}(u\cdot L)\,dF(u)=\int_0^1\tau_1^{\Delta\nu}\left[u(\xi)\cdot L\right]\,d\xi,\quad F\left[u(\xi)\right]=\xi,\quad \xi\in[0,1] \tag{6}$$

in which a non-constant positive scaling coefficient u is introduced. In Eq. (6), F is the distribution function of the variable u.

In quasi-scaling, we thus assume that the two spectra can be related to each other by a spectral scaling function which is statistically independent from at least one of the two spectra. Obviously, if the density of the distribution function F of variable u is a Dirac, this relationship provides the scaled model.

Defining explicitly the variable u is complicated in a general frame unless gas spectra follow rigorously the quasi-scaled property, which is rare (almost as rare as truly correlated gas spectra). However, application of the mean value theorem to Eq. (6) shows that for any gas path length L, there exists a particular value of the variable ξ, for which the corresponding scaling coefficient, that will be from now on written $u(L)$, is such that:

$$\tau_2^{\Delta\nu}(L) = \int_0^1 \tau_1^{\Delta\nu}\left[u(\xi)\cdot L\right]\, d\xi = \tau_1^{\Delta\nu}\left[u(L)\cdot L\right] \qquad (7)$$

The mean value theorem thus replaces the problem of specification of the distribution function of scaling coefficients, *F*, by an implicit equation that only involves as input data the uniform transmissivities. As these transmissivities are usually known (but their functional form depends on the uniform model selected), the application of the quasi-scaling assumption is always possible. This property of Godson's method was already emphasized in ref. [11]. It should be noticed that the implicit formulation of the quasi-scaling approximation is also similar to the definition of the strictly increasing function that relates the spectra in C*k* / CKD method: in both cases, the explicit link between the spectra does not need to be fully specified, only its existence is assumed and its effect is formulated through an implicit relationship.

The implicit equation set by Eq. (7) can be solved easily using the formalism introduced recently in the ℓ-distribution approach and briefly reminded in the next section.

3. FROM GODSON'S METHOD TO L-DISTRIBUTION

It is out of the scope of the present paper to fully redevelop the set of equations related to the ℓ-distribution approach. Interested readers can find a comprehensive description of the technique in ref. [16]. We only remind here some of the most important results (Section 3.1) and show how, based on this general theory, one can propose simple though accurate estimate of narrow band transmissivities of high temperature gaseous paths (section 3.2). The simplified model, that involves three parameters, is first described in uniform cases and its extension to non-uniform paths is then detailed in Section 4. Several test cases in uniform scenarios are provided that illustrate the accuracy of the method when assessed against LBL calculations.

3.1. TABULATION OF UNIFORM LBL TRANSMISSIVITES IN THE L-DISTRIBUTION METHOD

The ℓ-distribution approach can be introduced as follows. Most LBL data are provided in terms of absorption coefficients. At high spectral resolution, LBL sets contain a large number of spectral values. In many applications: 1/ there is no real interest for high resolution data as only spectral averages (from narrow bands up to the full spectrum) gas radiative properties are needed. This is the case for heat transfer applications but also for radiative imaging studies in which the band width is fixed by the imaging device, and 2/ over spectral intervals, the integral form of the radiative transfer equation involves spectrally averaged transmissivities (weighted by the Planck function in the case of wide bands or over the full spectrum). Calculating these non-uniform transmissivities using LBL data requires a two-step process: 1/ (path integral) for each wavenumber inside the band, evaluate the sum of all contributions (sum of $\kappa_{\nu,i}\ L_i$) encountered along the path and, 2 / (spectral averaging) evaluate the non-uniform transmissivity by averaging all these spectral contributions.

Based on these observations, a real gain in terms of computational cost could be expected if one could tabulate directly LBL transmissivities since one part of the process (calculation of band averaged transmissivities from high resolution LBL data) required to solve the RTE would be avoided. In other words, if LBL transmissivities could be precalculated in advance, an important reduction of the computational cost could be

anticipated. This is the main idea behind the uniform model used in the ℓ-distribution method.

In order to tabulate LBL data in transmission form, we first generate an approximate model (formally the same as the SNB model for Lorentz lines using the Malkmus' distribution of linestrengths [9] and the second order *k*-moment model [21]) called in refs. [5,16] the "germ" model. Its coefficients are given by the set of equations (no optical filter is considered here – more general formula involving such an optical filter are provided in ref. [5]):

$$k_P = \frac{1}{\Delta\nu} \cdot \int_{\Delta\nu} \kappa_\nu \, d\nu \tag{8-a}$$

$$k_R^{-1} = \frac{1}{\Delta\nu} \cdot \int_{\Delta\nu} \frac{d\nu}{\kappa_\nu} \tag{8-b}$$

$$\beta = \frac{\pi}{k_P / k_R - 1} \tag{8-c}$$

Eqs. (8-a) and (8-b) are the definitions of the Planck and Rosseland mean absorption coefficients of the gas over the spectral band $\Delta\nu$ respectively. Eq. (8-c) is a parameter that measures the overlapping between spectral lines. Indeed, it coincides exactly with the overlapping parameter of the SNB model for Lorentz lines with Malkmus' distribution of linestrengths if the real gas spectrum follows rigorously the assumptions of this SNB model [9].

As can be seen from the definitions (8.a-c), all the parameters involved in the "germ" model can be evaluated as simple integrals over the absorption coefficients taken from a LBL dataset.

Then, one can notice that the germ model (all quantities related to the "germ" model are, as in ref. [5], represented by an index "0") is invertible and its inverse is analytical. The direct model and its inverse are given respectively as:

$$\tau_0^{\Delta\nu}(L) = \exp\left[-\frac{\beta}{\pi} \cdot \left(\sqrt{1 + \frac{2\pi k_P L}{\beta}} - 1 \right) \right] \tag{9-a}$$

$$\Lambda_0^{\Delta\nu}(X) = \frac{\beta}{2\pi k_P}\cdot\left[\left(1-\frac{\pi}{\beta}\ln X\right)^2 - 1\right] \qquad (9\text{-b})$$

By definition, the inverse $\Lambda_0^{\Delta\nu}$ is such that:

$$\Lambda_0^{\Delta\nu}\left[\tau_0^{\Delta\nu}(L)\right] = L \qquad (10)$$

The LBL transmissivity in the gas is defined as:

$$\tau^{\Delta\nu}(L) = \frac{1}{\Delta\nu}\cdot\int_{\Delta\nu}\exp\left(-\kappa_\nu L\right)\, d\nu \qquad (11)$$

Using Eq. (10), we can rewrite this equation as:

$$\tau^{\Delta\nu}(L) = Gr\left[\tau_0^{\Delta\nu}(L)\right] \qquad (12)$$

where, for any X in [0,1]:

$$Gr(X) = \frac{1}{\Delta\nu}\cdot\int_{\Delta\nu}\exp\left[-\kappa_\nu\ \Lambda_0^{\Delta\nu}(X)\right]\, d\nu \qquad (13)$$

The *Gr* function, named the mapping function: 1/ establishes a direct relationship between the values of the germ model and the exact LBL values, 2/ maps the unit interval into itself and is strictly increasing (and thus invertible). This function can be tabulated easily (it suffices to discretize the unit interval into *N* subintervals and apply the definition of the *Gr* function Eq. (13) to generate a look-up table of *Gr* values). This direct tabulation method was applied in refs. [5,16,22].

3.2. SIMPLIFIED L-DISTRIBUTION MODEL

The main drawback of the ℓ-distribution method is its memory cost if high resolution *Gr* look-up tables are used (typically, 1000 values of *X* inside [0,1] are used, ensuring an accuracy on the calculation of transmissivities much lower than 10^{-3} in uniform calculations [16]). The size of the databases used in the "standard" high temperature version, already applied in ref. [22], is given in table 1. These databases contain model parameters for 28 gas temperatures (from 300 K up to 3000 K by 100 K step) for CO_2, CO and H_2O. For H_2O, 9 values of molar fractions (0., 0.05, 0.1, 0.2, 0.3, 0.4, 0.6, 0.8, 1.0) are used. Only atmospheric pressure is considered here.

Molecule	CO_2	CO	H_20
Number of molar fractions	1	1	9
Number of temperatures	28	28	28
Number of spectral bands	449	194	998
Size of the look-up table (Mb)	393.4	170.0	7869.1

Table 1. "Standard" parameters used in the building of ℓ-distribution databases (each *Gr* function uses 1000 values inside [0,1]) and the same number is used for the inverse of *Gr* which is also tabulated – the number of molar fractions and temperatures is fixed by the LBL database provided in ref. [23]. Only atmospheric pressure is considered here.

In order to reduce the memory cost of the technique, we propose in the following a simple though accurate method to approximate the mapping functions (and their inverse) required in the model.

Based on the visualization of mapping functions (see for instance the figures provided in refs. [5,16]), we propose to approximate the mapping functions by simple one parameter power functions, i.e.:

$$Gr(X) = X^{\lambda} \tag{14}$$

In this case, their inverses remain simple:

$$Gr^{-1}(X) = X^{1/\lambda} \tag{15}$$

Consequently, using this simple model, one can condense 2000 values for the *Gr* function and its inverse, each based on look-up tables containing 1000 single values for each of these functions, into a single coefficient λ. Parameters λ are obtained in this work as solutions of the non-linear least square problem (that only involves one single variable,

so that any numerical method can be used to perform this minimization – in the present work, the bisection method was used to solve Eq. (16)):

$$\lambda = \lambda_0 \text{ such that } \frac{\partial}{\partial \lambda_0}\left\{\int_0^1 \left[X^{\lambda_0} - Gr(X) \right]^2 dX \right\} = 0 \tag{16}$$

This minimization problem is solved for all states in the initial model database. The size of the simplified model database after this treatment for the same molecules, set of temperatures and species concentrations used in Table 1 are given in Table 2. In the same table, the size of the CKD model for 16 gray gases is also provided for comparison.

Molecule	CO_2	CO	H_20
Simplified ℓ-distribution	0.6 Mb	0.3 Mb	12.3 Mb
CKD (16 gray gases)	5.3 Mb	1.81 Mb	81.1 Mb

Table 2. Size of the look-up tables for CKD and simplified ℓ-distribution models - the same sets of thermophysical states and spectral bands as used in table 1 are considered.

Once the coefficients λ are estimated, uniform gas path transmissivities can be evaluated as:

$$\tau^{\Delta\nu}(L) = \exp\left[-\frac{\lambda\beta}{\pi} \cdot \left(\sqrt{1 + \frac{2\pi k_P L}{\beta}} - 1 \right) \right] \tag{17}$$

that follows directly from Eqs. (9-a, and 14). Their inverse is then:

$$\ell(X) = \frac{\beta}{2\pi k_P} \cdot \left[\left(1 - \frac{\pi}{\lambda\beta} \ln X \right)^2 - 1 \right] \tag{18}$$

For two states (subscripts 1 and 2), the two previous relationships provide function $\ell_1 \circ \tau_2^{\Delta\nu}(L)$ as required in the propagative scheme of Eq. (5) as:

$$\ell_1 \circ \tau_2^{\Delta\nu}(L) = s^2 \cdot \frac{k_{P,2}\,\beta_2}{k_{P,1}\,\beta_1} \cdot L + s \cdot \frac{k_{P,2}}{k_{P,1}} \cdot \left(1 - s \cdot \frac{\beta_2}{\beta_1} \right) \cdot \frac{\beta_2}{\pi k_{P,2}} \cdot \left(\sqrt{1 + \frac{2\pi k_{P,2} L}{\beta_2}} - 1 \right) \tag{19}$$

where:

$$s = \frac{\lambda_2}{\lambda_1}\frac{\beta_2}{\beta_1} \tag{20}$$

This relationship generalizes Eq. (50) of ref. [5], that corresponds to the particular case s=1. It provides the solution to Eq. (7) as $u(L) = \frac{\ell_1 \circ \tau_2^{\Delta\nu}(L)}{L}$.

The set of equations (18-20) defines what will be called from now on the simplified ℓ-distribution method. Examples of application of the transmissivity model set by Eq. (17) in the case of uniform situations are provided in Figures 1 to 4. They are equivalent to Figures 1-3 and 10 of ref. [18]. In each figure, the model is assessed against LBL calculations averaged over 25 cm^{-1}, which is the width of the narrow bands used to generate the simplified ℓ-distribution model parameters used in Eq. (17). The comparisons between LBL and simplified ℓ-distribution results show an excellent agreement, with errors lower than 1% over most parts of the spectrum. The highest errors (they attain 2 percent) are observed in the band head of CO_2 near 2400 cm^{-1} in the case of figure 4. These errors are due to the rather complicated behavior of the mapping function Gr at this spectral location than does not allow a proper adjustment using a single exponent λ to provide more accurate results. On the same cases, the use of the full ℓ-distribution database provides absolute differences between LBL and the model of the order of 10^{-6}. This is the same order of magnitude as already observed in Figure 3 of ref. [16], and the results for this model are not provided again here. This high quality of the uniform ℓ-distribution model is fully related to its construction, which was shown to be a tabulation of LBL data in transmission form. The main source of errors is related to the interpolation of the look-up tables of the Gr functions, which is small when 1000 values are used over [0,1] as done in the present work. The simplified version developed here is noticeably less accurate, but the gain in terms of memory space is significant (see tables 1 and 2) and the order of magnitude of accuracy (of the order of 1%) appears sufficient for most radiative transfer calculations in high temperature gases. This level of accuracy in uniform cases is comparable with the SNB model described in ref. [18]. Notice that most of the equations provided here to treat non-uniform paths, which is the main focus of the paper, can be readily extended to the SNB model of [18], due to their strong formal similarities.

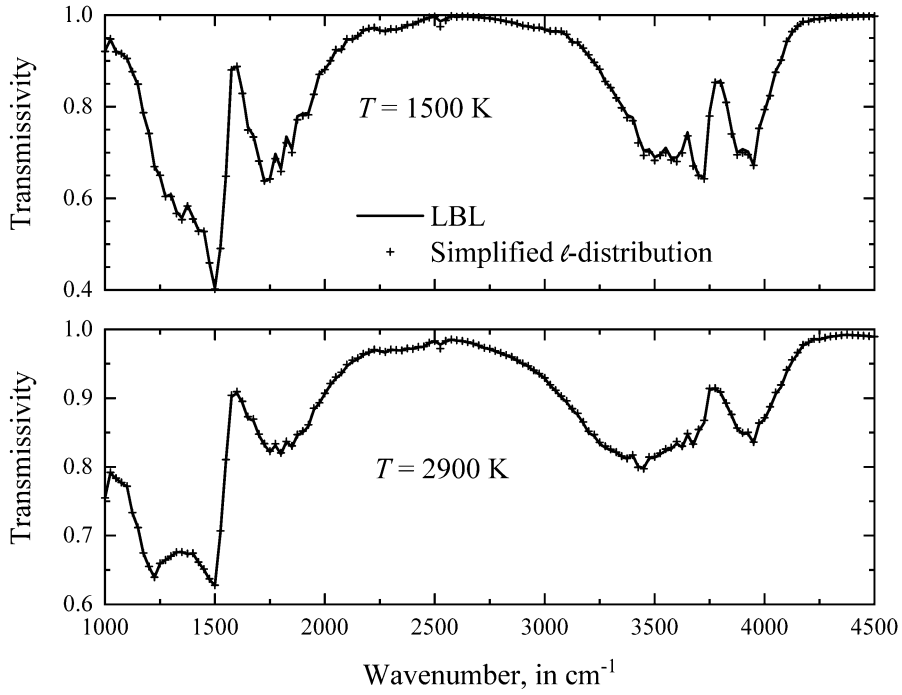

368

369 **Figure 1.** Transmissivities of H_2O-N_2 mixtures at 1500 K (top) and 2900 K (bottom)–

370 x_{H_2O} =0.1 - length *L*=10 cm – total pressure *P*=1 atm

371

372

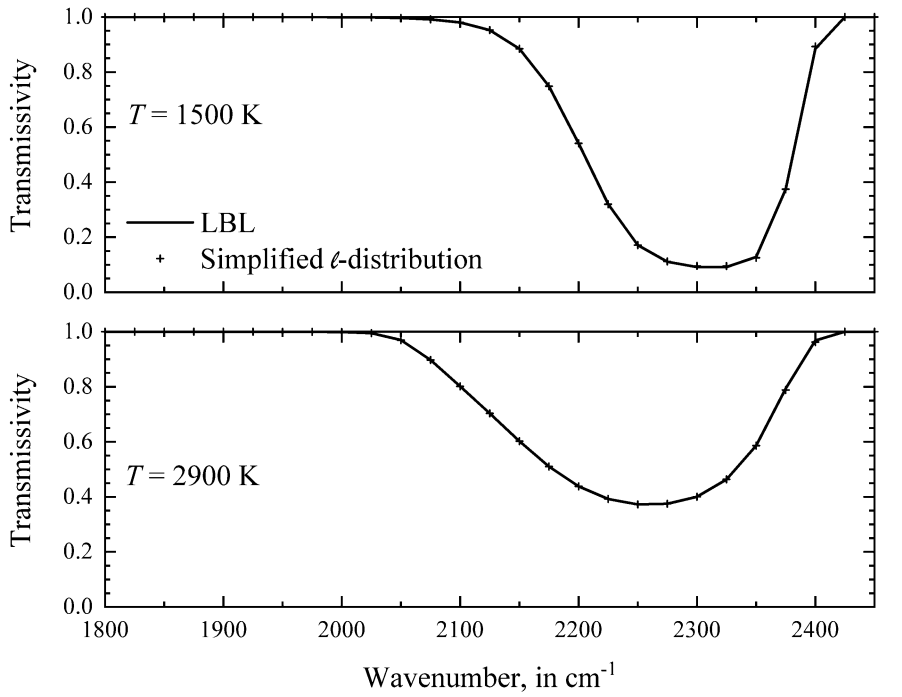

373

374 **Figure 2.** Transmissivities of CO_2-N_2 mixtures at 1500 K (top) and 2900 K (bottom) –

375 x_{CO_2} = 0.1 - length *L*=10 cm – total pressure *P*=1 atm

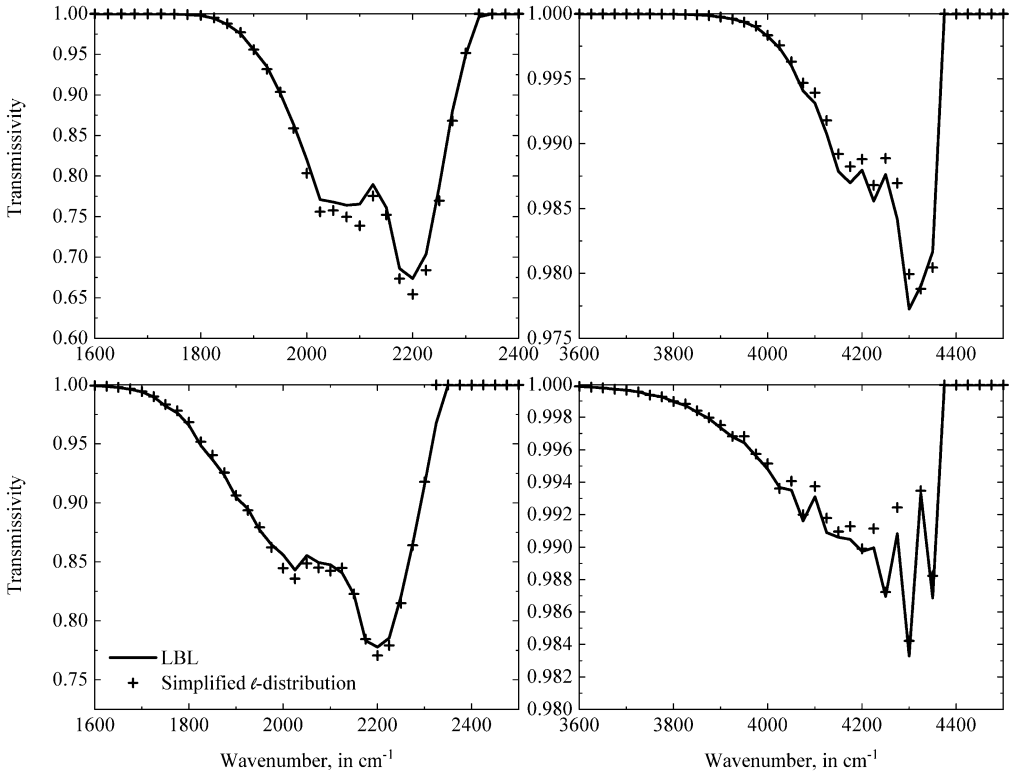

376

377 **Figure 3.** Transmissivity of CO-N_2 mixtures at 1500 K (top) and 2900 K (bottom) –

378 x_{CO_2} = 0.01 - length *L*=1000 cm – total pressure *P*=1 atm

379

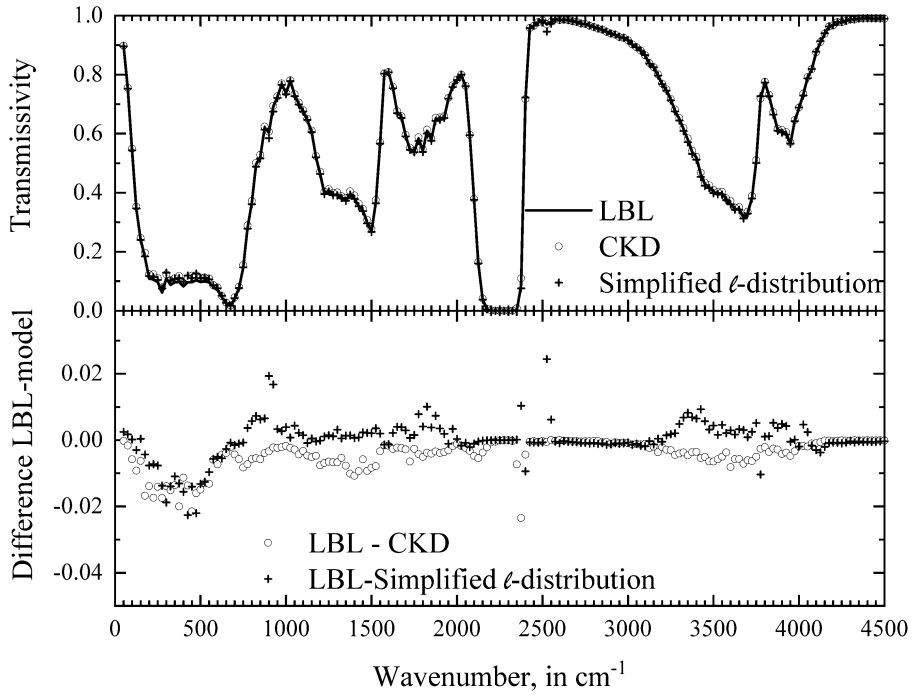

380

381 **Figure 4.** Transmissivity of a H_2O-CO_2-N_2 mixture with x_{H2O}=0.2 and x_{CO2}=0.1 at 2000 K

382 – length *L*=100 cm – total pressure *P*=1 atm (top) – Absolute difference / LBL (bottom)

4. FROM L-DISTRIBUTION TO RECURRENT NEURAL NETWORKS

Methods based on neural networks have received recently an increasing interest from various fields of applied physics and engineering, including the modeling of fluid flows, signal processing, etc. As noticed in ref. [4], their applications to radiative transfer problems remain in comparison very limited. Some of them were reminded in the introduction.

The aim of artificial neural networks is to mimic the processes involved in the human brain to learn information and to perform various tasks using computers (prediction, classification, recognition, etc). Most usual neural networks appertain to one of the two following main categories [24]:

- Static neural networks: the most usual type of static networks used is called feedforward. This kind of model mostly evaluates non-linear functions of its inputs.
- Dynamic neural networks: recurrent neural networks are classical examples of this kind of methods. In this case, the model is driven by non-linear time (in our case space, as will be shown later) dependent recurrent equations. Recurrent neural networks are founded on unit cells (of the same form as feedforward networks) for which some of the outputs (called state outputs) are fed back to its inputs after applying some time delay.

A cell (or neuron) is a non-linear bounded function of its inputs. It performs two main elementary operations: 1/ it first takes its inputs and evaluate a weighted sum of these variables, including a possible bias (constant) and 2/ the result of this linear model is then modified by an activation function to introduce non-linearities. There exist various types of activation functions: sigmoidal as used in ref. [4], hyperbolic tangent, rectified linear units (ReLUs, $\mathrm{ReLU}(x)=\mathrm{Max}[0,x]$) as applied in ref. [3], etc. Very often, at the exit of the activation function, a second stage of the same couple of processes (linear model fed into another activation function) is used, leading to the concept of hidden layer. Hidden layers perform intermediate computations that have an important role on the quality of the whole model, but do not produce values that have a direct interest for the modeler for which only the final outputs are of importance. Once the structure (number of weights and of hidden layers) is selected and all activation functions are specified, the training of the network mostly consists of estimating the set of weights that provides the

best approximation of a given training set by the neural network. Identification of the weights is made by application of optimization methods (more or less sophisticated least square fitting process). Once the weights are known, the neural network is usually assessed against a test set, that differs from the training dataset.

Based on this general framework, our aim is to show that the propagative scheme introduced in the previous sections can be rather naturally reformulated using an algorithm that is formally equivalent to a recurrent neural network. This type of structure has not been apparently considered up to now for generating fast transmission methods of gas radiation. However, RNN structures are usually good candidates to treat dynamical systems [25] and time series [26]. It is then not surprising to find the same form to be well adapted to sequences of path lengths, as encountered in the propagative scheme of Eq. (5). Here, we only focus on the simplified transmission model described in Section 3. This choice allows some simplifications and an analytical treatment which is sufficient for the purpose of the present work. Our objective is to explain why the selection of an RNN model for non-uniform gas radiation modeling is relevant, but not to propose a general formulation of non-uniform gas path models as RNNs. Extensions of the present developments to real LBL data are however discussed later in this section.

In section 4.1., we first present the concept of Exponential Linear Unit (ELU) introduced in ref. [27]. Among other, we explain why this choice of activation function inside an RNN structure is pertinent for non-uniform gas radiation modeling. In section 4.2., we show how the propagative scheme of Eq. (5) can be rewritten in terms of ELUs and discuss the corresponding algorithm. Its relationship to RNN is emphasized. Several test cases in non-uniform high temperature configurations are used to compare the "direct" ℓ-distribution method based on the uniform model of Section 3 together with the non-uniform treatment based on the RNN version of Eq. (19), derived in Section 4.2, against reference LBL calculations and a CKD model with 16 gray gases absorption coefficients. Multi-layer configurations involving mixtures of CO_2-H_2O-CO-N_2 at high temperature are considered for this purpose and results are detailed in Section 4.3. Finally, Section 4.4 provides a discussion of the present modeling strategy and explains how, based on previous works, it can be extended to real LBL datasets instead of the simplified model used here.

4.1. THE EXPONENTIAL LINEAR UNIT (ELU)

Activation functions are key components of artificial neural networks. For non-uniform gas radiation modeling, Exponential Linear Units (ELUs) have interesting properties. They are detailed here.

Exponential Linear Units were introduced recently [27] to be used as activation function in Neural Networks. Their application was found to speed up learning in deep neural networks and improve their classification accuracies. This activation function was shown in ref. [27] to outperform other activation functions on different vision datasets.

These units are similar to rectified linear units (ReLUs), initially introduced within the frame of Boltzmann machines [28]. Compared to ReLUs that are non-negative and thus have a mean activation larger than zero, ELU have a negative component, which decreases the so-called bias shift effect that consists of introducing some possibly artificial bias shift in the next units along the network. A bias shift is a constant that is added to the linear model (weighted average of the inputs) before to enter the activation function.

The Exponential Linear Unit with coefficient $\alpha > 0$ is defined as:

$$\varphi_\alpha(x) = \begin{cases} x \text{ if } x > 0 \\ \alpha\left(\exp(x) - 1\right) \text{ if } x \le 0 \end{cases} \tag{21}$$

In order to abridge the notations, we will use from now on the notation $\varphi(x) = \varphi_1(x)$.

Properties of ELU (derivative, etc) useful for the design of neural networks are provided in ref. [27]. The function $\varphi(x) = \varphi_1(x)$ is depicted in Figure 5. As can be seen, for negative values of the variable *x*, the ELU activation function converges slowly toward a negative value.

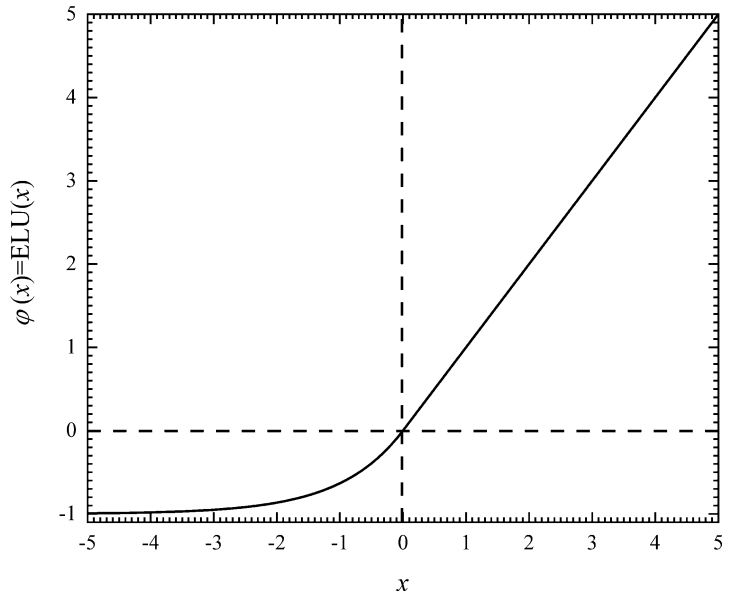

Figure 5. The Exponential Linear Unit (ELU)

The use of ELUs to model gas radiative properties is rather natural, if one notices that the emissivity of a gas path of length L in the gas is (here in Full Spectrum form):

$$\varepsilon(L) = \frac{\pi}{\sigma T^4}\int_0^{+\infty}\left[1-\exp\left(-\kappa_\nu L\right)\right] I_{b\nu}(T)\ d\nu = -\frac{\pi}{\sigma T^4}\int_0^{+\infty}\varphi\left(-\kappa_\nu L\right) I_{b\nu}(T)\ d\nu \qquad (22)$$

Many existing methods founded on gas path emissivities, including *k*-distribution and WSGG models for instance, can thus be considered technically as particular types of Neural Networks (of the projection pursuit form [29]) involving ELUs. As will be shown in the next section, the same ELUs can be used to treat path non-uniformities. For this purpose, we will show how formula Eq. (19) can be rewritten in terms of a two layer neural network based on ELUs. The resulting propagative scheme of Sections 2-3 will then be proved to be mathematically equivalent to an RNN constructed with the help of ELU activation functions.

4.2. REFORMULATION OF THE L-DISTRIBUTION PROPAGATIVE SCHEME AS A RECURRENT NEURAL NETWORK.

Conceptually, the propagative scheme used in the ℓ-distribution approach converts a sequence of geometrical gas path lengths $\{L_1,\ L_2,\ \ldots,\ L_n\}$ into another sequence of

equivalent absorption lengths $\{L_{1..n},\ L_{2..n},\ \ldots,\ L_{nn}\}$. These equivalent absorption lengths are defined by the recurrence relationships [5], as a generalization of Eq. (5) that is limited to two layers:

$$\begin{cases} L_{nn} = L_n \\ L_{i..n} = L_i + \ell_i \circ \tau_{i+1}^{\Delta\nu}\left(L_{i+1..n}\right) \end{cases} \tag{23}$$

As soon as the equivalent absorption path length $L_{1..n}$ is calculated, the transmissivity of the path $L_1 + L_2 + \ldots + L_n$ is then:

$$\tau_{1..n}^{\Delta\nu}\left(L_1,..,L_n\right) = \tau_1^{\Delta\nu}\left(L_{1..n}\right) \tag{24}$$

Any model can be used to calculate $\tau_1^{\Delta\nu}$. In the present work the uniform model of Eq. (17) is applied.

The propagative scheme can be written in the same form as an RNN, as depicted in Figure 6 for 3 layers (the general case is a direct generalization of this scheme). This requires each cell (circle) in the graph to evaluate a function of the form of $L_i + \ell_i \circ \tau_{i+1}^{\Delta\nu}\left(L_{i+1..n}\right)$. Obviously, this necessitates that $L_{n+1..n} = 0$, *i.e.*, the left input on the cell of the left (this input is not depicted in the figure) is 0.

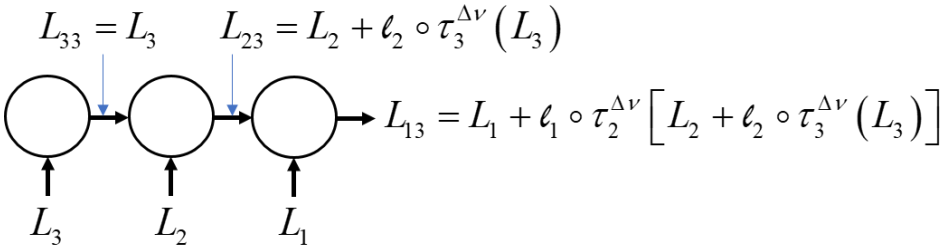

Figure 6. Architecture of a RNN equivalent to the propagative scheme – each cell (circle) calculates a function of the form $L_{i..n} = L_i + \ell_i \circ \tau_{i+1}^{\Delta\nu}\left(L_{i+1..n}\right)$.

In order to provide a direct reformulation of the propagative scheme of Figure 6 as an RNN written in terms of ELUs, we first notice that, using the same notations as in Eq. (19):

$$\left(1+\frac{2\pi k_{P,2}L}{\beta_2}\right)^{-1/2}=\frac{1}{\sqrt{\pi}}\cdot\int_0^{+\infty}y^{-1/2}\exp(-y)\cdot e^{-y\cdot\frac{2\pi k_{P,2}L}{\beta_2}}\,dy \tag{25}$$

If one then uses a Gauss-Legendre quadrature at order N over [0,1], and write $x_j,\ \ j=1,..,N$ and $\omega_j,\ \ j=1,..,N$ its nodes and weights respectively, it is easy to check that:

$$\left(1+\frac{2\pi k_{P,2}L}{\beta_2}\right)^{-1/2}\approx\sum_{j=1}^{N}\omega_j\cdot\exp\left(-u_j\cdot\frac{2\pi k_{P,2}L}{\beta_2}\right) \tag{26}$$

where coefficients $u_j,\ \ j=1,..,N$ are solutions of:

$$P\left(1/2\,;u_j\right)=x_j,\ \ j=1,..,N \tag{27}$$

in which:

$$P(a\ ;u)=\frac{1}{\Gamma(a)}\int_0^u t^{a-1}\exp(-t)\,dt \tag{28}$$

is the incomplete Gamma function [30]. In the present work, this function was evaluated with routines provided in ref. [31] and solutions of Eq. (27) were obtained using the bisection method.

Eq. (26) can then be integrated with respect to the gas path length between 0 and L to yield:

$$\sqrt{1+\frac{2\pi k_{P,2}L}{\beta_2}}-1\approx-\frac{1}{2}\cdot\sum_{j=1}^{N}\frac{\omega_j}{u_j}\cdot\varphi\left(-u_j\cdot\frac{2\pi k_{P,2}L}{\beta_2}\right) \tag{29}$$

This quantity corresponds to the last term at the RHS of Eq. (19). Based on this last relationship together with Eq. (19), we can eventually formalize the process in each of the cells of figure 6 in terms of ELUs. This is depicted in figure 7.

The specification of the weights that appear in the RNN model of Eq. (29) and figure 7 mostly consists of the evaluation of the quantities $u_j,\ \ j=1,..,N$. This means that solving Eq. (27) is equivalent to a learning stage as it provides all the weights required in the model. Additional details on this learning stage and on its extension to the case of real LBL data instead of the simplified model used here are provided later in section 4.4.

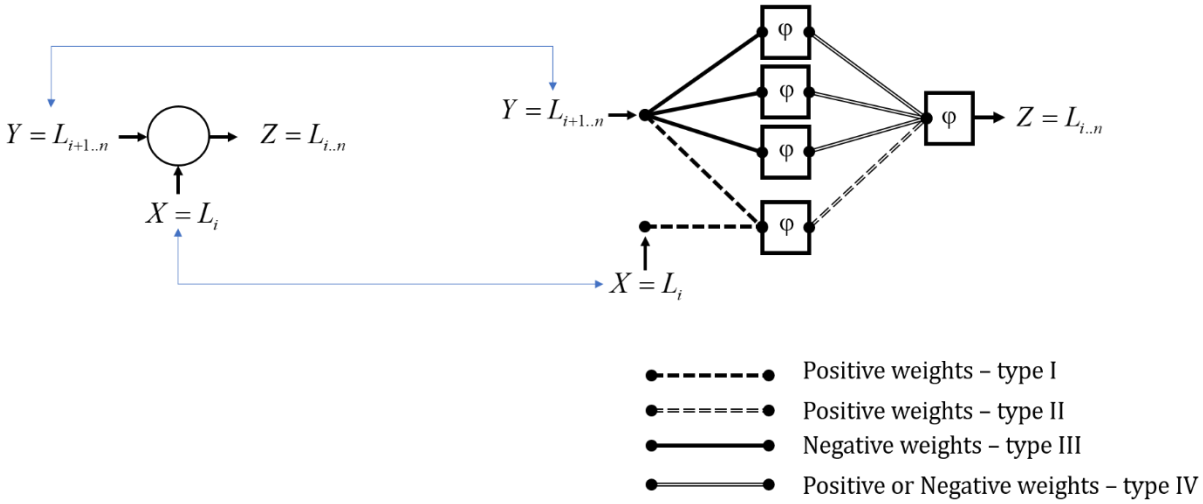

Figure 7. Details on the cells (circles) involved in Figure 6 for *N*=3

As shown in figure 7 (where the quadrature order *N* is 3, which explains the number of squares at the top of figure 7. In the case of a general quadrature order *N*, the total number of squares in figure 7 would be *N*+2), 4 types of weights are used (they follow directly from Eqs. (19,20,26)):

- type I weights are of the form: $\left\{1, s_i^2 \frac{k_{P,i+1}}{k_{P,i}} \frac{\beta_{i+1}}{\beta_i}\right\}$. This branch combines its two inputs L_i and $L_{i+1..n}$ to calculate $L_i + s_i^2 \cdot \frac{k_{P,i+1}}{k_{P,i}} \frac{\beta_{i+1}}{\beta_i} \cdot L_{i+1..n}$ (related to the first term at the RHS of Eq. (19)).

- type III weights are of the form: $-u_j \cdot \frac{2\pi k_{P,i+1}}{\beta_{i+1}}$. At the exit of the three squares on the top of figure 7, we thus have $\varphi\left(-u_j \cdot \frac{2\pi k_{P,i+1} L_{i+1..n}}{\beta_{i+1}}\right) = \exp\left(-u_j \cdot \frac{2\pi k_{P,i+1} L_{i+1..n}}{\beta_{i+1}}\right) - 1$

- type IV weights are of the form $-s_i \cdot \frac{k_{P,i+1}}{k_{P,i}} \cdot \left(1 - s_i \cdot \frac{\beta_{i+1}}{\beta_i}\right) \cdot \frac{\beta_{i+1}}{2\pi k_{P,i+1}} \cdot \frac{\omega_j}{u_j}$. These weights can be positive or negative, depending on the sign of the quantities inside the brackets. In case of strong gradients of temperatures and species concentrations, it was shown in ref.

549 [17] that negative weights should be preferred, requiring possibly a reorganization of
550 the treatment of the layers along the path as explained in ref. [5]. In the test cases
551 considered here and detailed in the next section, only small gradients of temperature
552 and species concentrations are considered between successive layers and this possible
553 problem of asymmetries is not further discussed.

554 - type II weight is 1.

555 Based on these relationships, one can readily check that at the output of each cell, each
556 of which being equivalent to a feedforward neural network whose state output [24] is
557 $Z = L_{i..n}$, we receive exactly the same quantity as calculated through Eq. (19). This proves
558 the equivalence between the iterative scheme of Eq. (5) and the graphical algorithm set
559 by figures 6 and 7. Obviously, the use of this algorithm in the case of the simplified
560 transmission model of section 3 is questionable, as an analytical solution, provided by
561 Eq. (19), exists. But its application to more general gas path transmissivities based on
562 LBL calculations instead of the simplified model of Section 3.2 is possible, as studied in
563 ref. [17]. This extension is discussed later, in section 4.4. Examples of application in non-
564 uniform configurations for various choices of the order of the quadrature *N* are provided
565 in the next section. They illustrate the relevance of the proposed methodology and
566 validate the applicability of the formulation in terms of recurrent neural network in
567 radiative transfer applications.

568 **4.3. APPLICATION IN NON-UNIFORM CONFIGURATIONS**

569 Test cases of the simplified ℓ-distribution model in uniform configurations were already
570 provided in section 3, and shown to yield excellent accuracy when assessed against LBL
571 calculations. In the present section, we evaluate the same model both against reference
572 LBL calculations and a CKD model with 16 gray gases based on a Gauss-Legendre
573 quadrature. For the CKD model, the double (in cases of mixtures of CO_2, H_2O and N_2) and
574 triple (in cases of mixtures of CO_2, CO, H_2O and N_2) integration methods were used to
575 treat mixtures of absorbing species. Here, we only focus on the accuracy of the non-
576 uniform model so that the use of these schemes to handle mixtures in the CKD method is
577 acceptable. However, in order to provide details on the calculation costs and make a fair
578 comparison of the methods in terms of CPU time, a specific version of the CKD model
579 was also written to allow application of the uncorrelated assumption of transmissivities

[9] to treat mixtures of absorbing species. This CKD model is only used for this CPU time analysis as it provides exactly the same results as the method described earlier, but was restricted to binary mixtures of absorbing species (instead of three for the CKD model described earlier). Results are provided in Table 3 in the case C1 (non-isothermal mixture of CO_2 and H_2O) detailed below, with 200 uniform sub-layers along a non-uniform path. The CPU times corresponds to 10^5 single narrow band (including both CO_2 and H_2O absorption) calculations. The simplified ℓ-distribution model is thus about 2.5 time more efficient than the CKD model with 16 gray gases.

Model	CPU time
CKD with 16 gray gases	25 s
ℓ-distribution	15 s
Simplified ℓ-distribution	11 s

Table 3. CPU time comparisons for 10^5 single narrow band calculations (200 uniform sub-paths per non-uniform ray).

As profiles of temperatures and species concentrations are considered in the following cases, a few words about the interpolation technique used in the simplified ℓ-distribution method are needed. This model depends on 3 coefficients, as shown in Eq. (17). The first two coefficients are mean (Planck and Rosseland) absorption coefficients of the gas. These coefficients are interpolated to any state not included in the database linearly with respect to the temperature in the CO and CO_2 cases, bi-linearly with respect to temperature and H_2O molar fraction in the case of water vapor. The same linear and bi-linear schemes were used for λ. This very simple method will be shown to provide accurate results in the test cases considered in this study.

The first two non-uniform cases (C1 and C2) were taken from ref. [22] (C1) and ref. [32] (C2) respectively. Case C3 was proposed recently by Wang in ref. [33]. Based on this configuration, two total path lengths (C3: 10 cm and C4: 100 cm) are considered. In all cases, non-uniform paths are divided into 200 uniform sub-paths and the same discretization is used for all gas radiation methods. Radiative intensities are evaluated at the location $l=L$. Concerning the simplified ℓ-distribution model, its two formulations are evaluated: the first one will be referred to as its direct formulation, based on Eq. (19) to

607 treat non-uniformities; the second one will be called RNN and is based on the
608 formulation described in section 4.2. Various orders of quadrature N (see Eqs. (26-29)),
609 from 4 (results for a quadrature order of 1 are of poor quality, reason why they are not
610 provided here) up to 256 are used for the comparisons between the direct model and its
611 RNN reformulation. Line of sight (0D) calculations are performed.

612 **4.3.1. Case C1**

613 In case C1, the profiles of temperature and species concentrations are given as:

$$\begin{cases} T(l) = 700\ \text{K} - 300\ \text{K} \times \cos\left(\dfrac{\pi l}{L}\right) \\ x_{H_2O}(l) = 0.2 - 0.15 \times \cos\left(\dfrac{\pi l}{L}\right) \\ x_{CO_2}(l) = \dfrac{2}{3} x_{H_2O}(l) \end{cases} \tag{30}$$

615 where the total distance of the path is L=300 cm.

616 Results are depicted in Figure 8. All subsequent figures (from 8 to 11) use the same
617 structure. On the top, radiative intensities in W/m^2/sr calculated LBL and averaged over
618 narrow bands (25 cm^{-1}) are provided. In the middle, the difference between the LBL
619 intensity and its approximate model value (either based on CKD or simplified ℓ-
620 distribution) divided by the maximum value of narrow band averaged LBL intensity is
621 given. This choice was made to avoid possible divisions by small values in almost
622 transparent zones. At the bottom, differences (absolute value of the difference between
623 band averaged intensities, in log-scale) between the direct non-uniform model and its
624 RNN approximation for various orders of the quadrature N are given.

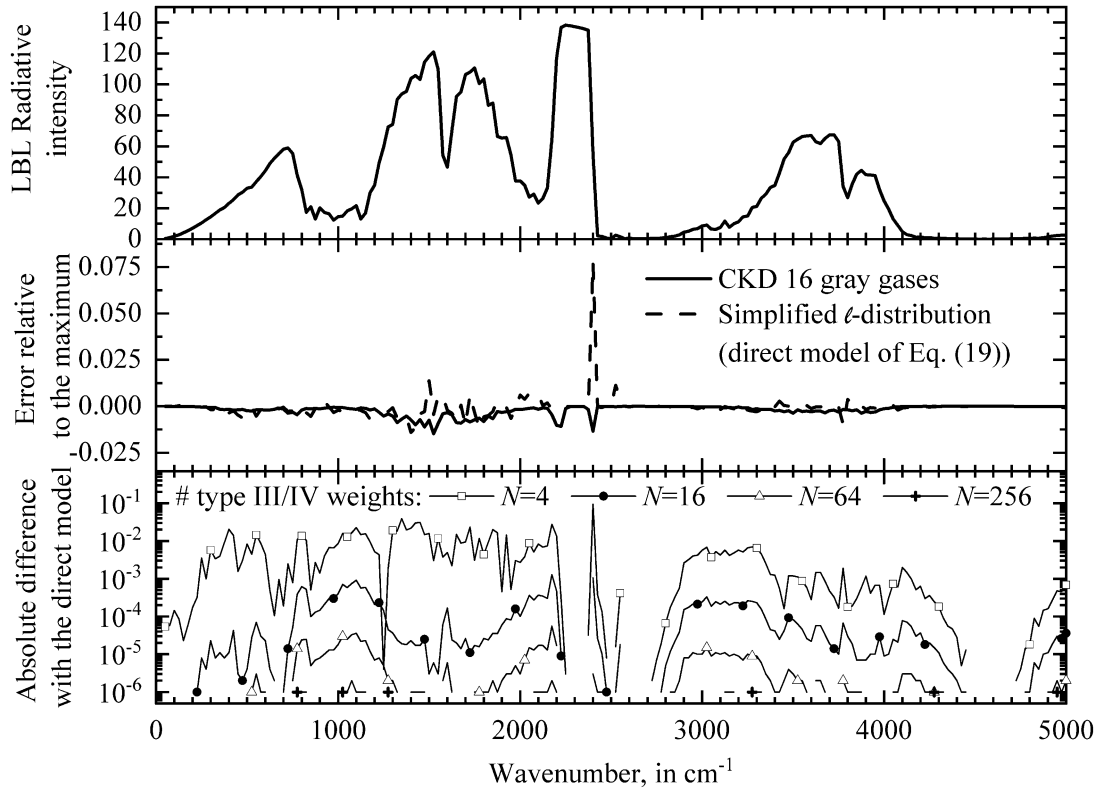

625

626 **Figure 8.** Intercomparison of radiative intensities in Case C1.

627 From Figure 8, one can notice that the overall quality of the simplified ℓ-distribution
628 method is comparable with the CKD model. Only at 2400 cm^{-1}, in the band head of CO_2,
629 errors are above 2%, for the same reasons as in the cases of section 3.2. In terms of total
630 intensity, the LBL model provides 6925 $W.m^{-2}.sr^{-1}$, 6870 $W.m^{-2}.sr^{-1}$ (0.8 % / LBL) for
631 CKD and 6910 $W.m^{-2}.sr^{-1}$ (0.2 % / LBL) for the direct simplified ℓ-distribution model. For
632 N=16, the difference between the direct model and its RNN version is lower than 0.02
633 $W.m^{-2}.sr^{-1}$ for the calculation of the total intensity.

634 **4.3.2. Case C2**

635 The profiles of temperature and species concentrations used in case C2 are given as:

$$\begin{cases} T(l) = 400\ \mathrm{K} + 1400\ \mathrm{K} \times \left[\sin\left(\dfrac{\pi l}{L} \right) \right]^2 \\ x_{H_2O}(l) = 0.4 \times \left[\sin\left(\dfrac{\pi l}{L} \right) \right]^2 \\ x_{CO_2}(l) = \dfrac{1}{2} x_{H_2O}(l) \end{cases} \tag{31}$$

636

where the total distance of the path is L=100 cm.

Results are depicted in figure 9. The same conclusions as in case C1 can be made. A quadrature order of N=4 provides large errors and the choice N=16 yields small though noticeable differences when compared with the direct model. There errors remain minor, especially when averaged over the full spectrum. Indeed, in terms of total radiative intensities, LBL calculation provides 18919 W.m^{-2}.sr^{-1}, CKD 19667 W.m^{-2}.sr^{-1} (4 % / LBL) the direct simplified ℓ-distribution model 19184 W.m^{-2}.sr^{-1} (1.4 % / LBL). The difference with its RNN version with N=16 is lower than 0.4 W.m^{-2}.sr^{-1} when summed over the full spectrum. It is below 0.001 W.m^{-2}.sr^{-1} when the quadrature order N=256 is used.

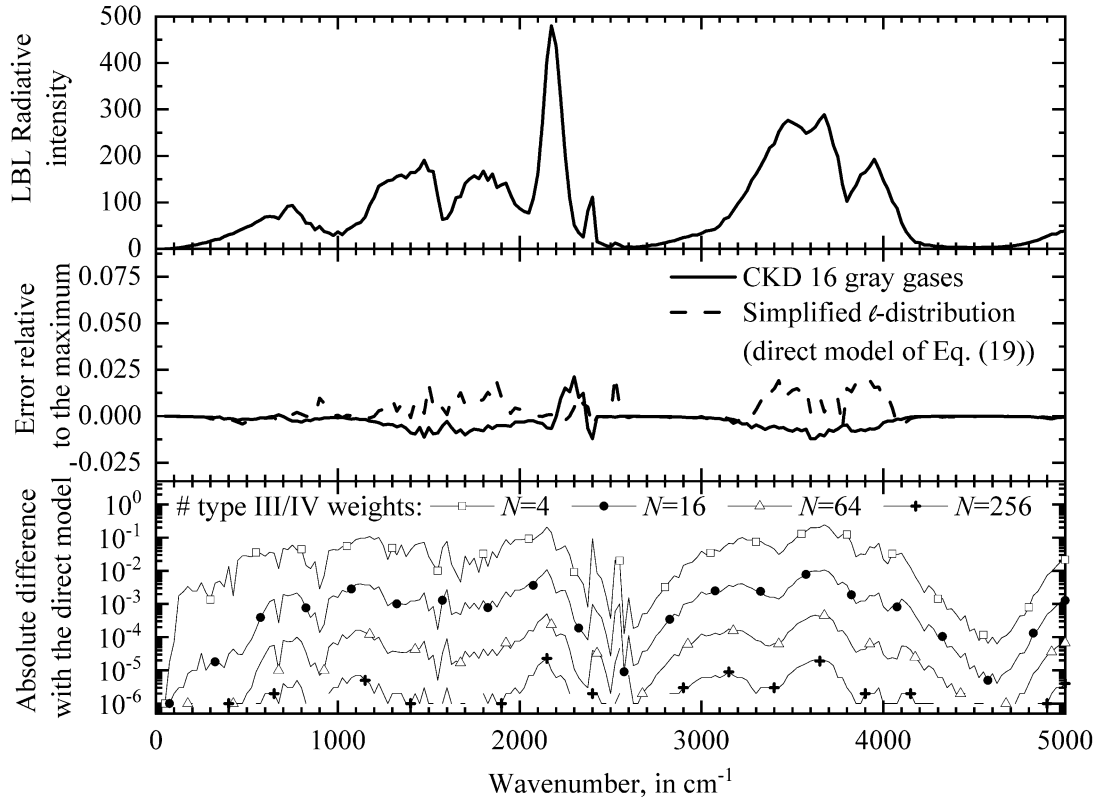

Figure 9. Intercomparison of radiative intensities in Case C2.

4.3.3. Cases C3 and C4

Case C3 uses the following profiles of temperature and species concentrations:

651
$$T(l) = \begin{cases} 1500.0 \sin\left(\frac{5\pi}{3}\frac{l}{L} + \frac{\pi}{4}\right), & 0 \le l \le 0.3 \\ 6798.76 \exp\left(-7.3\frac{l}{L}\right), & 0.03 \le l \le L \end{cases} \quad \text{(32-a)}$$

652
$$x_{H_2O}(l) = \begin{cases} 0.1 \sin\left(2\pi\frac{l}{L} + \frac{\pi}{4}\right), & 0 \le l \le 0.025 \\ 0.34 \exp\left(-6.28\frac{l}{L}\right), & 0.025 \le l \le L \end{cases} \quad \text{(32-b)}$$

653
$$x_{CO_2}(l) = \begin{cases} 0.1 \sin\left(\frac{10\pi}{7}\frac{l}{L} + \frac{\pi}{4}\right), & 0 \le l \le 0.035 \\ 0.34 \exp\left(-4.49\frac{l}{L}\right), & 0.035 \le l \le L \end{cases} \quad \text{(32-c)}$$

654
$$x_{CO}(l) = \begin{cases} 0.02 \sin\left(\frac{10\pi}{3}\frac{l}{L} + \frac{\pi}{4}\right), & 0 \le l \le 0.015 \\ 0.068 \exp\left(-10.47\frac{l}{L}\right), & 0.015 \le l \le L \end{cases} \quad \text{(32-d)}$$

655 where the total gas path length is first (case C3) L = 10 cm, which complies with the
656 value used in ref. [33]. Compared to the previous cases that were restricted to mixtures
657 of two absorbing molecules, 3 absorbing species are considered here (CO_2, H_2O and CO).
658 Predictions for this case are shown in Fig. 10.

659 In terms of total radiative intensities, LBL calculation provides 1202 W.m^{-2}.sr^{-1}, CKD
660 1167 W.m^{-2}.sr^{-1} (2.9 % / LBL), the direct simplified ℓ-distribution model 1179 W.m^{-2}.sr^{-1}
661 (1.9 % / LBL). The difference with its RNN version with N=16 is lower than 0.01 W.m^{-2}.sr^{-1}
662 for the calculation of the total intensity. It is below 0.00001 W.m^{-2}.sr^{-1} when N=256
663 is used.

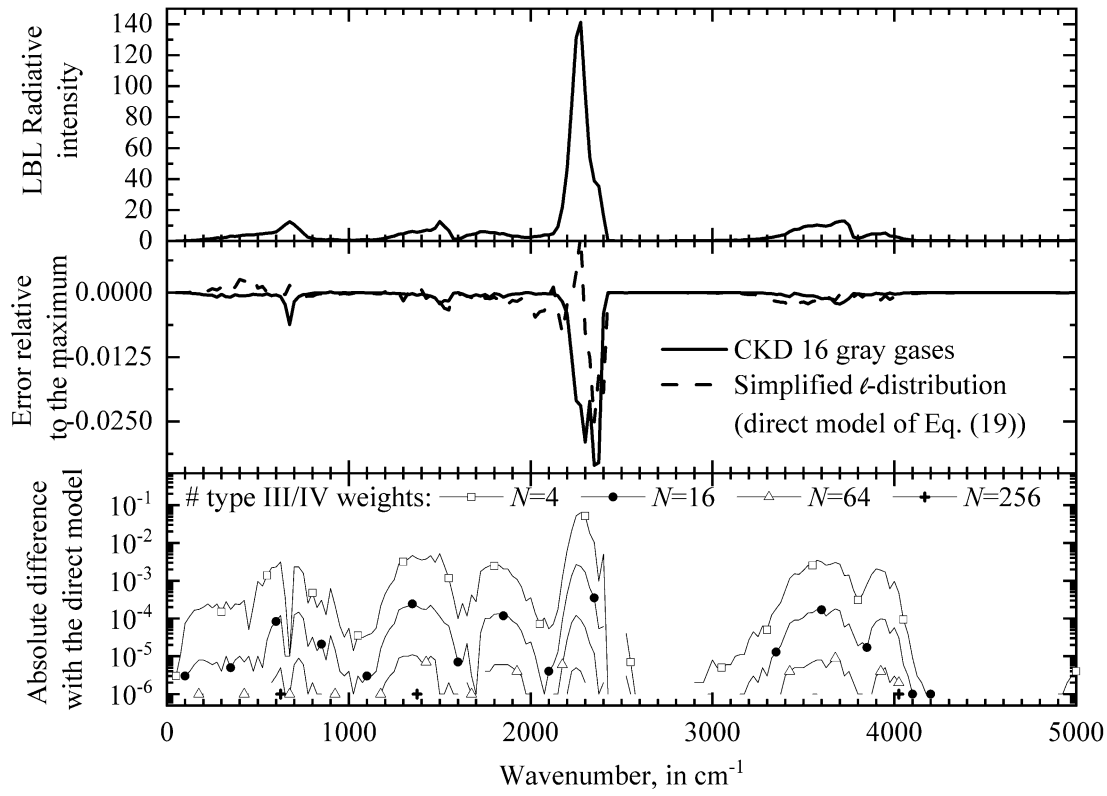

664

665 **Figure 10.** Intercomparison of radiative intensities in Case C3.

666 Case C4 is exactly the same as case C3 but the total length of the path is 100 cm. Results
667 are plotted in Figure 11.

668 In terms of total radiative intensities, LBL calculation provides 10261 $W.m^{-2}.sr^{-1}$, the CKD
669 model 10002 $W.m^{-2}.sr^{-1}$ (2.5 % / LBL), the direct simplified ℓ-distribution model 10337
670 $W.m^{-2}.sr^{-1}$ (0.7 % / LBL). The difference between the direct model and its RNN version
671 with N=16 is lower than 0.08 $W.m^{-2}.sr^{-1}$. It is below 0.0002 $W.m^{-2}.sr^{-1}$ for the calculation
672 of the total intensity when N=256 is used.

673

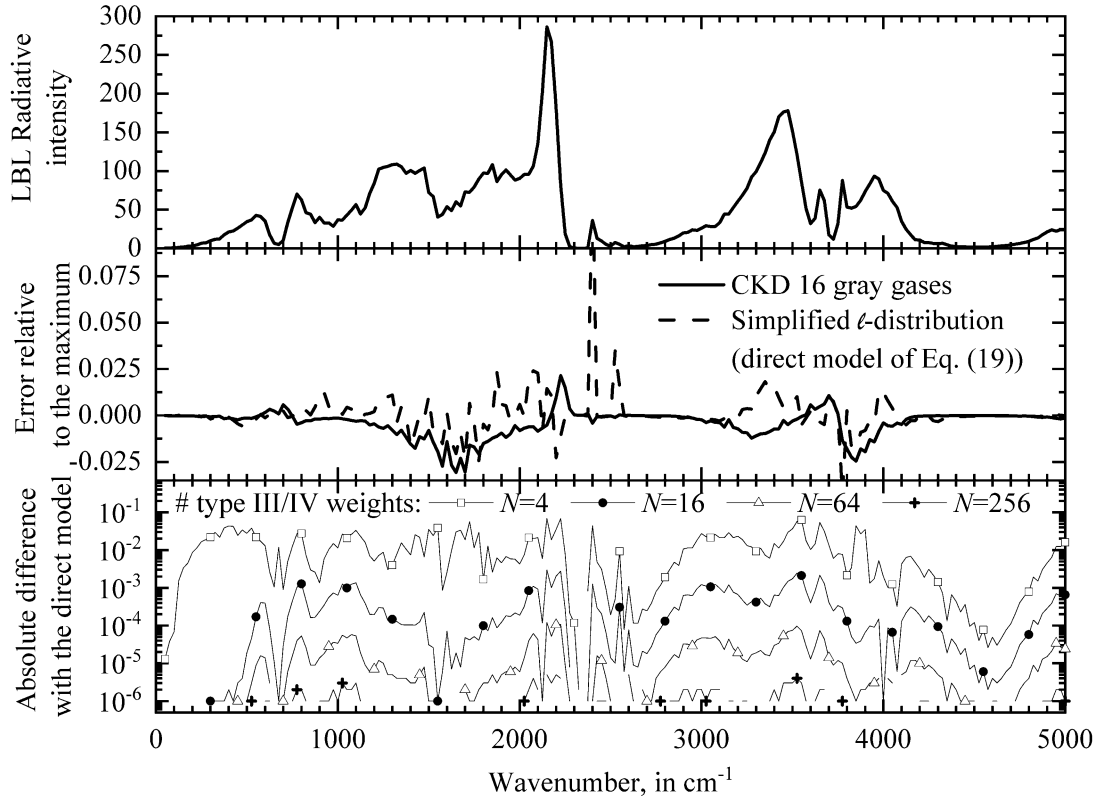

Figure 11. Intercomparison of radiative intensities in Case C4.

4.3.4. General comments on the non-uniform test cases

The set of test cases considered to evaluate both the direct and RNN versions of the propagative scheme set by Eq. (5) are limited but cover in fact a wide range of possible configurations. Indeed, these cases both involve optically thin and thick limits, wide ranges of values of mean absorption coefficients k_p and overlapping parameters β. These cases are thus sufficient to validate the RNN version of the propagative scheme proposed in this paper, which is the main focus of the present work.

With a quadrature order equal to N=4, large errors are observed (empty squares in figures 8 to 11). For values of N equal or higher than 16 (plain circles in figures 8 to 11), the RNN models almost coincide exactly with the one based on a direct application of the analytical formula Eq. (19). The same value of quadrature order N=16 was used in ref. [17] to treat real LBL data instead of the uniform model of Eq. (17). High temperature spectra were also considered in this work. This means that other quadrature orders may

be needed for atmospheric applications. The treatment of cases C1-4 however provides a proof of the actual possibility to treat non-uniform paths using the RNN structure depicted in Figures 6 and 7.

Moreover, the simplified ℓ-distribution model described in this paper has an accuracy which is similar to (and in all the considered cases higher than) the widely used CKD model for the calculation of full spectrum intensities. Considering its small memory cost and its high computational efficiency (the direct model is fully based on Eqs. (17,19), that only involve simple and analytical formulas), this method can be considered as a good candidate for radiative transfer applications in high temperature gaseous media. Its RNN version can be confidently used too, as it provides with a quadrature order of 16 almost the same accuracy as the direct method. Notice however that the RNN version is more computationally demanding than Eq. (19). A ratio of about 4 in terms of computational time was observed when the RNN version with N=16 is used instead of the direct model.

4.4. DISCUSSION

As noticed earlier in this paper, using the "neural" version depicted in Figures 6-7 to evaluate equivalent absorption lengths has probably little interest in the case of the uniform transmissivity model proposed in Section 3, since for this model these equivalent absorption lengths are analytical. They are indeed provided by Eq. (19). However, the present developments pave the way for further fast transmissivity model developments based on Recurrent Neural Networks, a structure that has not be considered yet to the best of the authors' knowledge. This point is discussed in this section.

The training of NN models is subject to known issues [29]. The choice of the starting values (how to initialize the weights?), overfitting (how to select the optimal number of weights?), and the choice of the structure of the network (how to select the number of hidden units and of layers?) are critical in the definition of the model. Choosing these parameters is difficult in a general frame. Indeed, as NN are most often black box models, it is almost impossible to specify all these quantities in advance. There are several tricks to circumvent these problems but, most of the time, trial and errors

techniques are used to select the best combination of parameters (structure, number of weights and initialization) [3].

Based on the present work, all these three issues can be solved if one uses the recurrent structure described in this paper.

Concerning the structure of the network, it is fixed by the scheme depicted in figure 6. There is no reason to add any additional layer in the method. The choice of the activation function (ELU) is also rather natural. The same kind of formulation in terms of ELUs was used in ref. [17] in the case of real gas spectra. This property extends to any problem for which the Archimedean copula C_{11} that appears in Eq. (4) is of the Levy Subordinated type [34,35]. Direct models of Archimedean copula (not necessarily Levy Subordinated) based on neural networks can be found in ref. [36] but the method is more focused on copula models than the method described here.

Concerning the optimal number of weights, it is mostly related to the choice of the number *N* related to the Gauss-Legendre quadrature used in Eq. (27). In ref. [17], a Gauss-Legendre quadrature at order 16 was selected (the corresponding formulation of ref. [17] is reminded later in this section). As shown in section 4.3, this order of quadrature was found to provide accurate results here too. Notice however, that both the present work and ref. [17] are dedicated to high temperature configurations. This means that adaptation of this quadrature order *N* may be needed for applications in the atmosphere. A detailed analysis of this specific point in cases of atmospheric paths is kept as future work.

Concerning the learning stage and the initialization of the weights, additional details are described in this paragraph. It was shown in ref. [17], that if: 1/ the absorption spectrum in state 1 is gray i.e., $\kappa_{\nu,1} = k_{P,1}$, and 2/ the non-constant scaling coefficient between spectra in states 1 and 2 is bounded and takes values inside a small interval, *i.e.*, $u(\xi) \in [u_{\min}, u_{\max}]$, $\frac{u_{\max} - u_{\min}}{u_{\min}} << 1$, solutions of Eq. (7) take the form:

$$\ell_1 \circ \tau_2^{\Delta\nu}(L) = u_{\min} L + \frac{1}{k_{P,1}} \cdot \int_0^{u_{\max} - u_{\min}} \left[1 - \exp\left(-k_{P,1} \cdot \mathrm{v} \cdot L\right)\right] dF(\mathrm{v}) \tag{33}$$

where $\mathrm{v} = u - u_{\min}$ and $F(\mathrm{v})$ is the distribution function of variable v over the spectral interval $\Delta\nu$. Eq. (33) can be rewritten as:

$$\ell_1 \circ \tau_2^{\Delta\nu}(L) = u_{\min} L + \frac{\overline{\mathrm{v}}}{k_{P,1}} \cdot \int_0^{u_{\max}-u_{\min}} \left[\frac{1 - \exp\left(-k_{P,1} \cdot \mathrm{v} \cdot L\right)}{\mathrm{v}} \right] dF^*(\mathrm{v}) \tag{34}$$

where $\overline{\mathrm{v}} = \int_0^{u_{\max}-u_{\min}} \mathrm{v}\, dF(\mathrm{v})$ is the mean value of v and $F^*(\mathrm{v}) = \frac{1}{\overline{\mathrm{v}}} \int_0^{\mathrm{v}} \mathrm{v}'\, dF(\mathrm{v}')$. Noticing that as v is positive by definition, $F^*(\mathrm{v})$ is a probability distribution function (its inverse will be from now on written v^*), one can rewrite Eq. (34) as:

$$\ell_1 \circ \tau_2^{\Delta\nu}(L) = u_{\min} L + \frac{\overline{\mathrm{v}}}{k_{P,1}} \cdot \int_0^1 \left[\frac{1 - \exp\left(-k_{P,1} \cdot \mathrm{v}^*(\xi) \cdot L\right)}{\mathrm{v}^*(\xi)} \right] d\xi \tag{35}$$

Using the same Gauss-Legendre quadrature as in section 4.2 to estimate the integral over [0,1], Eq. (35) can be approximated by:

$$\ell_1 \circ \tau_2^{\Delta\nu}(L) \approx u_{\min} L - \frac{\overline{\mathrm{v}}}{k_{P,1}} \cdot \sum_{j=1}^{N} \frac{\omega_j}{\mathrm{v}^*(x_j)} \cdot \varphi\left[-k_{P,1} \cdot \mathrm{v}^*(x_j) \cdot L\right] \tag{36}$$

that takes exactly the same functional form as used in 4.2.

Moreover, in the same reference [17], it was verified in real LBL cases that this formulation can be extended to non-gray cases by simply replacing the mean absorption coefficient $k_{P,1}$ of Eqs. (33-36) by some moment of the absorption coefficient written μ_s. The general solution of Eq. (7) thus takes the form, similar to Eq. (35):

$$\ell_1 \circ \tau_2^{\Delta\nu}(L) = u_{\min} L + \frac{\overline{\mathrm{v}}}{\mu_s} \cdot \int_0^1 \left[\frac{1 - \exp\left(-\mu_s \cdot \mathrm{v}^*(\xi) \cdot L\right)}{\mathrm{v}^*(\xi)} \right] d\xi \tag{37}$$

that one can approximate, using again a Gauss-Legendre quadrature at order *N*, as:

$$\ell_1 \circ \tau_2^{\Delta\nu}(L) \approx u_{\min} L - \frac{\overline{\mathrm{v}}}{\mu_s} \cdot \sum_{j=1}^{N} \frac{\omega_j}{\mathrm{v}^*(x_j)} \cdot \varphi\left[-\mu_s \cdot \mathrm{v}^*(x_j) \cdot L\right] \tag{38}$$

Eqs. (37,38) provide the solution of Eq. (7) in the case of real LBL data. Eq. (38) takes exactly the same form as the one considered in 4.2. A table of correspondence between the quantities that appear in Eqs. (19,29) and Eq. (38) is provided in table 4.

Eq. (19,29)	**Eq. (38)**	**Physical meaning**
$\frac{2\pi k_{P,2}}{\beta_2}$	μ_s	Mean (moment) absorption coefficient
$s^2 \cdot \frac{k_{P,2}\ \beta_2}{k_{P,1}\ \beta_1}$	$u_{\min}$	Minimum value of scaling coefficient – corresponds to the asymptotic limit of the scaling function at large lengths *L*.
$s \cdot \frac{k_{P,2}}{k_{P,1}}$	$\overline{u}$	Mean value of scaling coefficient – corresponds to the asymptotic limit of the scaling function at small lengths *L*.
$s \cdot \frac{k_{P,2}}{k_{P,1}} \cdot \left(1 - s \cdot \frac{\beta_2}{\beta_1}\right)$	$\overline{\mathrm{v}} = \overline{u} - u_{\min}$	Mean value of coefficient v
u_j	$\mathrm{v}^*(x_j)$	Characterize the variations of scaling coefficients inside $[u_{\min}, u_{\max}]$

Table 4. Relationship between the quantities that appears in Eqs. (19,29) and Eq. (38)

This means that in the general case, the same algorithm as used in section 4.2 can be used. In practice, as detailed in ref. [17], several of the quantities that appear in Eq. (38) need to be adjusted on the LBL transmission curves because if the quasi-scaling approximation is close to the real behavior of gas spectra, it is not exact. This minimization process is equivalent to a training or learning stage in the machine learning terminology. The quantities that are adjusted on the LBL transmission curves, or equivalently learned from the LBL transmission curves, are essentially the parameters $\mathrm{v}^*(x_j),\ \ j = 1,..,N$ as soon as the coefficient μ_s is chosen (notice that the

exact specification of this coefficient μ_s is not compulsory as it always appears in formula (38) as the product $\mu_s \cdot \mathrm{v}^*(x_j)$ and coefficients $\mathrm{v}^*(x_j),\ j = 1,..,N$ are adjusted – this property arises from the change of distribution from F to F^* between Eq. (33) and Eq. (34)). From table 4, one can see that the training of coefficients $\mathrm{v}^*(x_j),\ j = 1,..,N$ in the LBL case is equivalent to the choice of coefficients $u_j,\ j = 1,..,N$ in the simplified ℓ-distribution model. The specification of these coefficients as solutions of Eq. (27) is thus the same as some training stage. No explicit learning step appears in the simplified ℓ-distribution approach because an explicit solution can be found but this learning stage is required when the methodology is applied to real LBL datasets. Combining the results described in the present paper with those of ref. [17] (or equivalently Eqs. (37,38)) thus provides all the elements required to generate an RNN model of non-uniform path transmissivities. This RNN model then has the interesting property that all its weights have a clear physical meaning, as detailed in table 4, avoiding the black box disadvantage of this category of methods. The parameters of the simplified ℓ-distribution model, or the same steps as described in ref. [17], can be used to initialize the optimization of the parameters of Eq. (38) on real LBL datasets.

Furthermore, both feedforward and recurrent neural networks are so-called universal approximators [25]. Accordingly, in theory, both of them are likely to estimate any non-uniform path transmissivity. However, the RNN architecture has some advantages compared to feedforward models. They are briefly discussed here. The iterative process proposed in this work can be readily adapted to any dimension (number of sub-paths encountered along a non-uniform path) which makes it appropriate for the treatment of general radiative transfer problems for which many such uniform sub-paths may be encountered along a ray. This iterative structure thus appears to be well suited to radiative transfer calculations, in comparison with any other feedforward networks as considered in ref. [4]. Indeed, in actual radiative transfer problems, the dimension of the input space (number of sub-paths along a ray) can quickly become difficult to handle if a large number of such inputs is treated. This would require the specification of many weights in feedforward NN models. In practice, large numbers of weights complicate the training of the model and reduce its computational efficiency compared to a LBL calculation. The propagative scheme introduced here does not suffer from this limitation

since only transitions between successive layers are modeled, *i.e.*, even in the case of a high number of sub-paths, what is modeled remains in dimension 2, as shown in figures 6 and 7.

Eventually, if the model presented in this work has some advantages compared to other methods for non-uniform path radiative transfer calculations, it also has some limitations. In fact, it can be noticed that the present method provides a gas radiation model formulated in terms of transmissivities. This type of formulation, whose main interest is to produce a fast model as no spectral or pseudo-spectral loop is required, has an impact on the possible choices of RTE solvers. Indeed, the present developments are limited to ray-tracing RTE solvers, which includes Monte Carlo methods but also quasi-Monte Carlo (qMC, [37]) techniques, *i.e.*, numerical methods based on the integral form of the RTE. The present model cannot be used with the Discrete Ordinate Method, for instance, as it uses the differential form of the RTE. However, the present modeling strategy can be applied for coupled calculations to treat engineering problems, in the same way the CKD model is used in refs. [38,39]. Compared to a combination of qMC and CKD, the use of the present model has one dimension less than CKD (no sampling or loop over gray gases) which can be beneficial to reduce the cost of a qMC calculation. Application of the simplified ℓ-distribution method together with a net exchange formulation is also as straightforward as it is for the SNB models [40]. Notice that one part of the justification of the copula formalism is founded on this idea of net exchange, as detailed in ref. [5], illustrating the strong theoretical connection between the present method and net exchange RTE solvers. In these contexts (ray tracing RTE solver and/or net exchange formulation), as shown in the paper, the "direct" simplified ℓ-distribution model can be used confidently. Furthermore, as pointed out several times in the paper, the "neural" version has little interest in the case of the simplified ℓ-distribution model but the present paper provides a proof of concept. The "neural" version may find application in problems for which only a finite set of transitions between layers (*i.e.* distinct states of the gas) needs to be considered in which case, the LBL formulation described two paragraphs above can be used instead of the simplified model of section 3.2. Indeed, the quantities that are trained in the RNN version are related to transitions between successive layers so that the number of parameters to identify is directly proportional to the amount of distinct states encountered in the problem. This kind of

configuration is relatively rare in high temperature configurations, for which the "direct" simplified ℓ-distribution model can be used, but rather usual in atmospheric sciences (multi-layer atmospheres). Application of the present developments in their recurrent neural network version for radiative transfer studies in the atmosphere, mostly as a continuation of ref. [5] and in which LBL datasets will be used instead of the simplified ℓ-distribution model considered in the present paper, is scheduled as future work.

5. CONCLUSION

The main objective of the work was to show that recurrent neural network models are relevant candidates for modeling non-uniform gas path transmissivities. Relationships between a method proposed by Godson in the 50s and RNNs, two a priori strongly distinct ideas, follow from a mathematical analysis and a reformulation of Godson's implicit equation. This reformulation involves the inverse of the transmission function. It provides an analytical method for the treatment of non-uniform paths. Most results provided here follow directly from recent results obtained within the frame of the development of the ℓ-distribution approach.

A simplified version of the ℓ-distribution method was introduced. The main advantage of this simplified model is that it allows a fully analytical derivation of all model parameters. Compared with the full database (that requires a few gigabytes), the size of the simplified ℓ-distribution model is lower than 14 megabytes. This method was found to be accurate both in uniform and non-uniform scenarios. Its accuracy of a few percent is sufficient for most radiative heat transfer calculations in high temperature gases.

Based on simple analytical developments, it was then shown that the propagative scheme associated with the ℓ-distribution method can be written in an RNN form. Indeed, this propagative scheme consists of a transformation of a series of optical paths into equivalent absorption lengths. The structure of the problem is well suited to RNN models, more usually encountered in the modeling of dynamical systems or the treatment of time series. The RNN formulation, that uses Exponential Linear Units (ELUs) as activation functions, was compared with the analytical solution and found to provide highly accurate estimates of non-uniform path transmissivities. All the weights involved in the RNN formulation have a clear physical meaning. This allows a high level of control and interpretability of the RNN model, a property which is usually hard to ensure with methods purely based on machine learning. The only quantities involved in the RNN model that are not directly related to the uniform model (the set of u_j) are obtained here as solutions of an implicit equation instead of a minimization process. This possibility is related to the choice of the simplified model for the calculation of transmissivities that allows a simplified treatment of the training of the model, but the process is equivalent to a learning stage. Extension of the method to real LBL

transmissivities instead of the simplified model was discussed. Future works will be devoted to its application for atmospheric calculations.

AKNOWLEDGEMENTS

This work was supported by the French National Research Agency under the grant ANR-20-CE04-0005 ASGARD.

889 **REFERENCES**

890

891 [1] ROYER A., FARGES O., BOULET P., BUROT D. A new method based on artificial neural
892 network for radiative heat transfer calculation: comparison with benchmark numerical
893 solutions in homogeneous media, in: *Proceedings of the International Symposium on*
894 *Advances in Computational Heat Transfer* (CHT-20), Rio de Janeiro, Brazil, 2020.

895 [2] MISHRA S., MOLINARO R. Physics informed neural networks for simulating radiative
896 transfer, *JQSRT*, Vol. 270, 2021, 107705.

897 [3] ZHOU Y., WANG C., REN T. A machine learning based efficient and compact full-
898 spectrum correlated k-distribution model, *JQSRT*, Vol. 254, 2020, 107199.

899 [4] STEGMANN P.G., JOHNSON B., MORADI I., KARPOWICZ B., McCARTY W. A deep
900 learning approach to fast radiative transfer, *JQSRT*, Vol. 280, 2022, 108088.

901 [5] ANDRE F., CORNET C., GALTIER M., DUBUISSON Ph. Radiative Transfer in the O_2 A-
902 band – A Fast and Accurate Forward Model Based on the ℓ-distribution Approach, *JQSRT*,
903 Vol. 260, 2021, 107470.

904 [6] GODSON W.L. The evaluation of infra-red radiative fluxes due to atmospheric water
905 vapor, *Q. J. R. Met. Soc.*, Vol. 79, 1953, pp. 367-379.

906 [7] GODSON W.L. The computation of infrared transmission by atmospheric water
907 vapor, *Journal of Meteorology*, Vol. 12, 1955, pp. 272-284.

908 [8] LINDQUIST G.H., SIMMONS F.S. A band model formulation for very nonuniform paths,
909 *JQSRT*, 1972, Vol. 12, pp. 807-820.

910 [9] YOUNG S.J. Band model theory of radiation transport, The Aerospace Press, 2013.
911 ISBN: 978-1-884989-25-4.

912 [10] YOUNG S.J. Evaluation of nonisothermal band models for H_2O, *JQSRT* 1977;18:29-
913 45.

914 [11] WEINREB M.P., NEUENDORFFER A.C. Method to apply homogeneous-path
915 transmittance models to inhomogeneous atmospheres, *J. Atm. Sci.* 1973;30:662-666.

[12] GORDLEY L.L., RUSSELL III J.M. Rapid inversion of limb radiance data using an emissivity growth approximation, *App. Opt.* 1981;20:807-813.

[13] GRIESSBACH S., HOFFMANN L., HÖPFNER M., RIESE M., SPANG R. Scattering in infrared radiative transfer: A comparison between the spectrally averaging model JURASSIC and the line-by-line model KOPRA, *JQSRT*, Vol. 127, 2013, pp. 102-118.

[14] MARSHALL B.T., GORDLEY L.L., CHU A.D. BANDPAK: Algorithms for modeling broadband transmission and radiance, *JQSRT*, Vol. 52, 1994, pp. 581-599.

[15] MODEST MF. Narrow-band and full-spectrum *k*-distributions for radiative heat transfer – correlated-*k* vs. scaling approximation, *JQSRT*, Vol. 76, 2003, pp. 69-83.

[16] ANDRE F. The ℓ-distribution method for modeling non-gray absorption in uniform and non-uniform gaseous media, *JQSRT*, Vol. 179, 2016, pp. 19-32.

[17] ANDRE F. Effective Scaling Factors in Non-uniform Gas Radiation Modeling, *JQSRT*, Vol. 206, 2018, pp. 105-116.

[18] RIVIERE Ph., SOUFIANI A. Updated band model parameters for H_2O, CO_2, CH_4 and CO radiation at high temperature, IJHMT, Vol. 55, 2012, pp. 3349-3358.

[19] NELSEN R.B. An introduction to Copulas - Second Edition, Springer series in statistics, Springer, 2006.

[20] JOE H. Multivariate models and dependence concepts, Monograph on statistics and applied probability 73, *Springer Science+Business Media* Dordrecht 1997.

[21] ANDRE F., VAILLON R. The *k*-moment method for modeling the blackbody weighted transmission function for narrow and wide band radiative properties of gases, *JQSRT*, Vol. 108, 2007, pp.1-16.

[22] ANDRE F., COELHO F., CONSALVI J.-L., FRANCA F.R.H., GALTIER M., NMIRA F., SOLOVJOV V.P., WEBB B.W. Accuracy of Engineering Methods for Radiative Transfer in CO_2-H_2O Mixtures at High Temperature, in RAD-19, *Proceedings of the Ninth International Symposium on Radiative Transfer,* Athens, Greece, eds. B.W. Webb and D. Lemonnier, Begell House, Connecticut, June 3-7, 2019.

[23] PEARSON J., WEBB B.W., SOLOVJOV V.P., MA J. Efficient Representation of the Absorption Line Blackbody Distribution Function for H_2O, CO_2, and CO at Variable Temperature, Mole Fraction, and Total Pressure, *JQSRT*, Vol. 138, 2014, pp. 82-96.

946 [24] DREYFUS G. Neural Networks – Methodology and Applications. Springer. 2005.

947 [25] SCHAFER A.M., ZIMMERMANN H.-G. Recurrent neural networks are universal
948 approximators, *International Journal of Neural Systems*, Vol. 17, 2007, pp. 253-263.
949 [26] HEWAMALAGE H., BERGMEIR C., BANDARA K. Recurrent neural networks for time
950 series forecasting, International Journal of Forecasting, Vol. 37, 2021, pp. 388-427.

951 [27] CLEVERT D.-A., UNTERTHINER T., HOCHREITER S. Fast and accurate deep network
952 learning by exponential linear units (ELUs), in: *Proceeding of the International*
953 *Conference on Learning Representation* (ICLR2016), 2016.

954 [28] NAIR V., HINTON G.E. Rectified linear units improve restricted Boltzmann machines,
955 in: *Proceeding of the 27th International Conference on Machine Learning* (ICML10), 2010.

956 [29] HASTIE T., TIBSHIRANI R., FRIEDMAN J. The Elements of Statistical Learning – Data
957 Mining, Inference, and Prediction – Second Edition. Springer. 2017.

958 [30] ABRAMOWITZ M., STEGUN I.A. Handbook of Mathematical Functions. Dover. 1965.

959 [31] Numerical recipes in Fortran 77: the art of scientific computing. Cambridge:
960 Cambridge University Press; 1992.

961 [32] COEHLO F.R., FRANCA F.H.R. WSGG correlations based on HITEMP2010 for gas
962 mixtures of H_2O and CO_2 in high total pressure conditions, *IJHMT*, Vol. 127, 2018, pp.105-
963 114.

964 [33] WANG C., MODEST M.F., REN T., CAI J., HE B. Comparison and refinement of the
965 various full-spectrum k-distribution and spectral line weighted-sum-of-gray-gases
966 models for nonhomogeneous media, *JQSRT*, Vol. 271, 2021, 107695.

967 [34] ANDRE F. An analysis of the symmetry issue in the ℓ-distribution method of gas
968 radiation in non-uniform gaseous media, *JQSRT*, Vol. 190, 2017, pp. 78-87.

969 [35] HERING C., HOFERT M., MAI J.-F., SCHERE M., Constructing hierarchical
970 Archimedean copulas with Levy subordinators, *J. Multivariate Analysis* 2010;101:1428-
971 1433.

972 [36] LING C.K., FANG F., ZICO KOLTER J. Deep Archimedean Copulas, in: *Proceedings of*
973 *the 34th Conference on Neural Information Processing Systems (NeurIPS 2020)*, 2020.

[37] LEMIEUX C. Monte Carlo and quasi-Monte Carlo sampling, *Springer Science+Business Media* Dordrecht 2009.

[38] PALLUOTTO L., DUMONT N., RODRIGUES P., KOREN C., VICQUELIN R., GICQUEL O. Comparison of Monte Carlo methods efficiency to solve radiative energy transfer in high fidelity unsteady 3D simulations, in: *Proceedings of Eurotherm Seminar 110 – Computational Thermal Radiation in Participating Media VI, April 11-13, 2018, Cascais, Portugal.*

[39] FARMER J., ROY S.P. A quasi-Monte Carlo solver for thermal radiation in participating media, *JQSRT*, Vol. 242, 2019:106753.

[40] CHERKAOUI M., DUFRESNE J.-L., FOURNIER R., GRANDPEIX J.-Y., LAHELLEC A. Monte Carlo simulation of radiation in gases with a narrow-band model and a net exchange formulation, *Journal of Heat Transfer*, Vol. 118, 1996, pp. 401-407.